

# X-ray fluorescence spectroscopy from ions at charged vapor/water interfaces

Wei Bu and David Vaknin

Ames Laboratory, and Department of Physics and Astronomy, Iowa State University, Ames, Iowa 50011, USA

(Dated: October 30, 2018)

X-ray fluorescence spectra from monovalent ions ( $\text{Cs}^+$ ) that accumulate from dilute solutions to form an ion-rich layer near a charged Langmuir monolayer are presented. For the salt solution without the monolayer, the fluorescence signals below the critical angle are significantly lower than the detection sensitivity and only above the critical angle signals from the bulk are observed. In the presence of a monolayer that provides surface charges, strong fluorescence signals below the critical angle are observed. Ion density accumulated at the interface are determined from the fluorescence. The fluorescent spectra collected as a function of incident X-ray energy near the  $L_{III}$  edge yield the extended absorption spectra from the ions, and are compared with recent independent results. The fluorescence data from divalent  $\text{Ba}^{2+}$  with and without monolayer are also presented.

PACS numbers: 61.10.Kw, 61.10.Ht, 73.30.+y 82.45.Mp

## I. INTRODUCTION

Recently, we reported on the spatial distributions of monovalent ions ( $\text{Cs}^+$ ) at highly charged interfaces at  $\sim 3$  Å resolution by using synchrotron x-ray anomalous reflectivity techniques<sup>1,2</sup>. We demonstrated that these distributions are well described by a Poisson-Boltzmann theory that accounts for proton release and binding to a  $\text{R-PO}_4\text{H}$  group (R is typically a fatty acid portion of the molecule). Subsequently, we reported on the extension of these studies by analyzing x-ray energy scans at fixed momentum-transfers ( $Q_z$ ) under specular reflectivity conditions. In addition to obtaining ion distributions, our analysis yielded the energy dependence of the dispersion corrections  $f'(E)$  and  $f''(E)$  near the  $\text{Cs}^+$   $L_{III}$  resonance<sup>3</sup>. This study confirmed the ion density accumulations at the charged interfaces and provided spectroscopic information of the ions with details that shed light on the immediate environment of the ions, similar to that obtained by extended x-ray absorption fine structure spectroscopy (EXAFS) experiments.

The x-ray fluorescence near total reflection is another common technique to determine ion adsorption to charged Langmuir monolayers at air/solution surface<sup>4-10</sup>. Herein, we report detailed determination of fluorescence spectra from monovalent ions  $\text{Cs}^+$  and divalent ions  $\text{Ba}^{2+}$ , both in solutions and as they form an ion-rich layer near the charged interfaces. We compare the findings with recent results obtained from the anomalous reflectivity technique<sup>1,2</sup>. In the present study, we extend on previous studies by exploring the fluorescence signals as a function of photon energies, in particular, near resonances. As shown below, our approach yields the energy dependence of the dispersion corrections of  $\text{Cs}^+$ ,  $f'(E)$  and  $f''(E)$ , near a resonance, which is known to be affected by the local non-crystalline environment of the ions. In the past, such corrections were obtained by Bijvoet Pairs at Bragg reflections<sup>11</sup>, by absorption cross-section measurements<sup>12,13</sup>, and by calculation using atomic wave functions<sup>14</sup>. In general, EXFAS and related spectroscopic experiments are conducted in transmission

configurations, but it is known that fluorescence experiments, as in this study, can yield similar results.

## II. EXPERIMENTAL SETUP AND METHODS

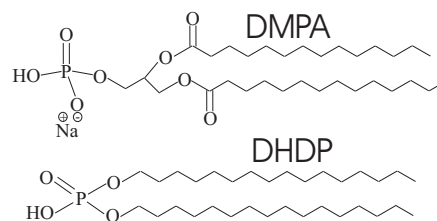


Figure 1: Dimyristoyl phosphatidic acid (DMPA) and dihexadecyl hydrogen phosphate (DHDP) molecules used to form the Langmuir monolayers.

To form well-controlled interfacial charges, monolayers of dimyristoyl phosphatidic acid (DMPA) and dihexadecyl hydrogen phosphate (DHDP) (Fig. 1) were spread at salt (e.g.,  $\text{CsI}$  and  $\text{BaI}_2$ ) solution/gas interfaces<sup>15-17</sup>. Detailed procedures of sample preparations and handling were described elsewhere<sup>1,2</sup>. Isotherms have been used for controlling the molecular area, fixed at  $41 \pm 1$  Å<sup>2</sup> in all discussed experiments. *In-situ* fluorescence spectra at the gas/liquid interface were conducted on the Ames Laboratory Liquid Surface Diffractometer at the Advanced Photon Source, beam-line 6ID-B (described elsewhere<sup>18</sup>). The highly monochromatic X-ray beam, selected by a downstream Si double crystal monochromator, is deflected onto the liquid surface at a desired angle of incidence with respect to the liquid surface by a second monochromator (y-cut quartz single-crystal  $d$ -spacing 4.25601 Å) mounted on the liquid-surface diffractometer yielding energy resolution  $\sim 0.85$  eV in the vicinity of the  $\text{Cs}^+$   $L_{III}$  resonances of the ions ( $\sim 5$  keV). The absolute scale of the x-ray energy was calibrated with various absorption edges to better than  $\pm 2$  eV. The incident photon energy can be continuously varied from 4 to 40

keV, in a fixed- $Q_z$  mode, namely, adjusting all angles to maintain fixed momentum transfer. Scattered photon intensities are normalized to an incident beam-monitor in front of the sample. Vortex-EX® Multi-Cathode X-Ray Detector (SII Nano Technology USA, Inc.), an energy-dispersive-detector (EDD), is lowered to the surface in an aluminum well with a thin Kapton window located  $\sim 2$  cm above the liquid surface (Fig. 2). The Langmuir trough is placed in a sealed canister kept under a flow of water-saturated helium gas.

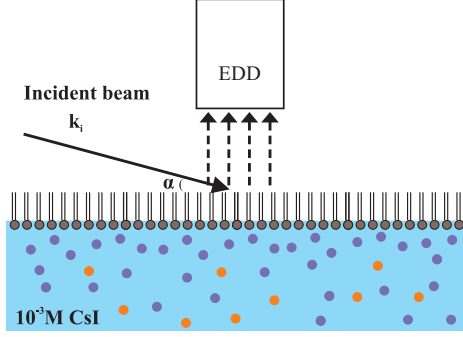


Figure 2: Illustration of the fluorescence experiment setup. The monolayer is spread in an encapsulated Langmuir trough purged with water saturated helium. The Vortex-EX® Multi-Cathode X-Ray Detector window (50 mm<sup>2</sup> effective detector area) is placed at a distance  $\sim 2$  cm from the surface. The fluorescent beam goes through a thin Kapton window that seals the trough.

Fluorescence is an ion-specific technique in that it can distinguish contributions from different ions because of their characteristic fluorescence spectra<sup>8–10,19</sup>. Since the x-ray penetration depth changes dramatically (from 60 – 80 Å to 1 – 2  $\mu$ m) around the critical angle ( $Q_c \sim 0.022$  Å<sup>-1</sup> for total reflection), the fluorescence signals below and above the critical angle for all solutions in the present study are dominated by different regions of the systems. Below the critical angle, the signal is less sensitive to contributions from the pure bulk solution and in the presence of charges is dominated by ions at the surface, due to the finite penetration depth of X-rays. On the other hand, above the critical angle, the fluorescence signals consist of contributions from the ions in the bulk and at the interface.

### III. RESULTS AND DISCUSSION

#### A. Surface ion enrichment

Figure 3 shows contour plots of fluorescence intensity as functions of X-ray photon energy,  $E$ , and momentum transfer,  $Q_z$ , for  $10^{-3}$  M CsI with and without DHDP monolayer. Without monolayer (upper panel), the fluorescence pattern is relatively simple. Below the critical angle ( $Q_z < Q_c$ ), no significant fluorescence intensity is observed, consistent with the fact that ions (e.g., Cs<sup>+</sup>,

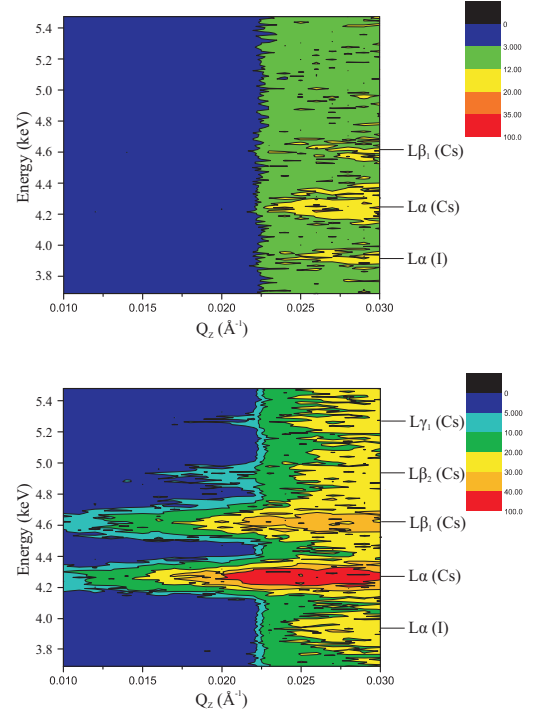


Figure 3: Contour plots of fluorescence intensity for  $10^{-3}$  M CsI without (upper panel) and with monolayer DHDP (lower panel). Emission lines are labeled on the right side. Incident x-ray beam energy is 8 keV.

I<sup>-</sup>) in the bulk are not concentrated enough to generate any detectable intensity over the very short penetration depth. For this ion concentration ( $10^{-3}$  M), we can practically claim that ions in the bulk have no contribution to the fluorescence signal in this  $Q_z$  range, or that for this concentration the signal from the surface (below the critical angle) is significantly lower than the sensitivity of our detector. This is true at least for dilute concentrations ( $10^{-3}$  M), but not for higher concentrations as shown below. Above the critical angle ( $Q_z > Q_c$ ), the x-ray beam penetrates much deeper (1 – 2  $\mu$ m), and this concentration is sufficient to generate fluorescence signals. A few main emission lines from Cs<sup>+</sup> ( $L\alpha$  and  $L\beta_1$ ) and I<sup>-</sup> ( $L\alpha$ ) are clearly identified. A general scheme defining the  $L$  shell emission lines is shown in Fig. 4. The fluorescence pattern with the DHDP monolayer (lower panel) is significantly different from that of the bare surface below the critical angle showing emission lines from Cs<sup>+</sup>, but none from I<sup>-</sup>. These emission lines include a few weaker ones ( $L\beta_2$  and  $L\gamma_1$ ), not observed from the bulk of the pure solution (upper panel). This is qualitative evidence that Cs<sup>+</sup> exclusively adsorb at the negatively charged surface, and no emission lines from I<sup>-</sup>, including the strongest  $L\alpha$ , are not observed below the critical angle. This is qualitative evidence that Cs<sup>+</sup> exclusively adsorb at the negatively charged surface. No emission lines from I<sup>-</sup>, including the strongest  $L\alpha$ , are observed

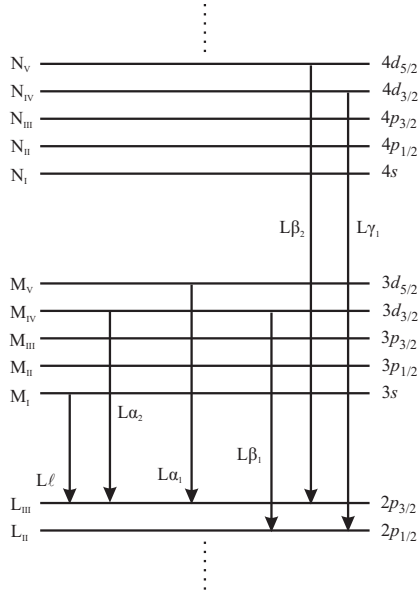


Figure 4: Schematic electron energy levels and main transition processes of the emission lines from the  $L$  shell.

below the critical angle. This implies that within the uncertainty of our measurement (about 0.1 ions per DHDP molecule) there is no enrichment of  $I^-$  at the interface. Using DMPA as a monolayer yields essentially the same fluorescence patterns (data not shown), consistent with theoretical predictions<sup>20</sup>.

Figure 5 (a) shows  $E$ -cuts (cuts along the energy axis at a specific  $Q_z$  value) of the fluorescence pattern for  $10^{-3}$  M CsI without the monolayer below ( $Q_z = 0.018 \text{ \AA}^{-1}$ ) and above the critical angle ( $Q_z = 0.030 \text{ \AA}^{-1}$ ). Fluorescence signals are observed only above the critical angle. In the presence of monolayers (DHDP and DMPA), the  $E$ -cuts below the critical angle are shown in Fig. 5 (b). As indicated, the emission lines from  $Cs^+$  are labeled, but no emission lines of  $I^-$  (e.g.,  $L\alpha$ ,  $\sim 3.9 \text{ keV}$ ) are detected. The DHDP or DMPA monolayers have practically identical fluorescence signals, which implies they have similar amounts of  $Cs^+$  ions at the surface. This is theoretically expected, according to the renormalized Poisson-Boltzmann theory<sup>2</sup>. This is because DHDP and DMPA have similar  $pK_a$  ( $\sim 2.1$ ) for the first proton release. At this concentration, it is not expected that the second hydrogen in DMPA will be released, unlike in the case of the divalent<sup>15</sup> or the trivalent ion solutions<sup>21</sup>.

Contour plots of fluorescence intensity for  $10^{-3}$  M CsI with and without the monolayer DHDP with incident x-ray beam energy at the Cs  $L_{III}$  resonance (5.015 keV), are shown in Fig. 6. The strong intensity ridge at approximately 5 keV is due to scattering of the incident beam, labeled as the primary beam. This signal consists of primarily elastic and Compton inelastic scattering. Figure 7(a) shows  $E$ -cuts obtained from Fig. 6 below the critical angle ( $Q_z = 0.018 \text{ \AA}^{-1}$ ). Because the incident beam energy is near the  $Cs^+$   $L_{III}$  resonance, only emission lines

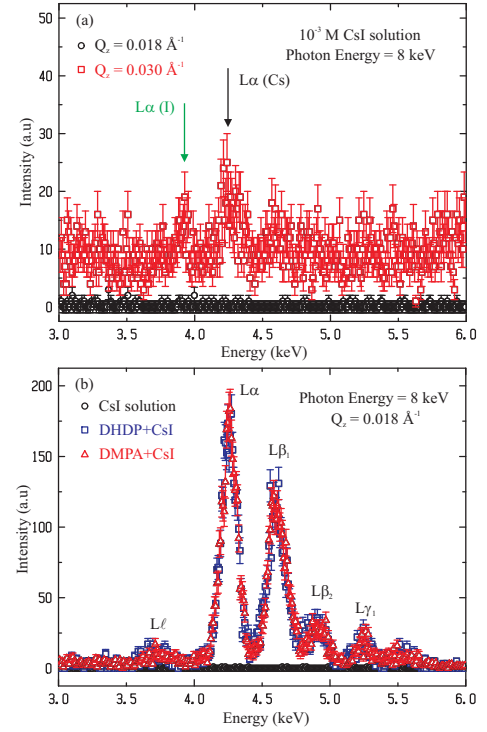


Figure 5: (a) Fluorescence intensity versus emission line energy for  $10^{-3}$  M CsI below and above the critical angle as indicated. (b) Fluorescence intensity versus emission line energy at  $Q_z = 0.018 \text{ \AA}^{-1}$  with and without monolayer at the interface.

from  $L_{III}$  ( $L\ell$ ,  $L\alpha$ ) are observed (the  $L\beta_2$  is entangled with the primary beam). Figure 7(b) shows the  $Q_z$ -cuts of  $Cs^+$   $L\alpha$  emission line from those contour plots. Without a DHDP or DMPA monolayer, the fluorescence signal is observed only above the critical angle, that is from the bulk. The intensity slightly increases with  $Q_z$  since the penetration depth becomes longer with  $Q_z$ <sup>6</sup>. With the DHDP monolayer, fluorescence intensity below the critical angle, due to surface enrichment of  $Cs^+$  at the surface is observed. This intensity reaches a maximum value at the critical angle, due to the multiple scattering, as predicted by the distorted wave Born approximation<sup>18,22,23</sup>.

Similar experiments performed with  $BaI_2$  solution (for  $10^{-2}$  M) with monolayers produce similar results. The fluorescence data below the critical angle with and without the DMPA monolayer are shown in Fig. 8. Because of the higher bulk concentration (than that used with CsI), the emission lines from both  $Ba^{2+}$  and  $I^-$  are observed below the critical angle for the bare surface solution without the monolayer. The presence of DMPA charges at the interface enhance the Ba emission lines, with no detectable change in the intensities of the  $I^-$  emission lines.

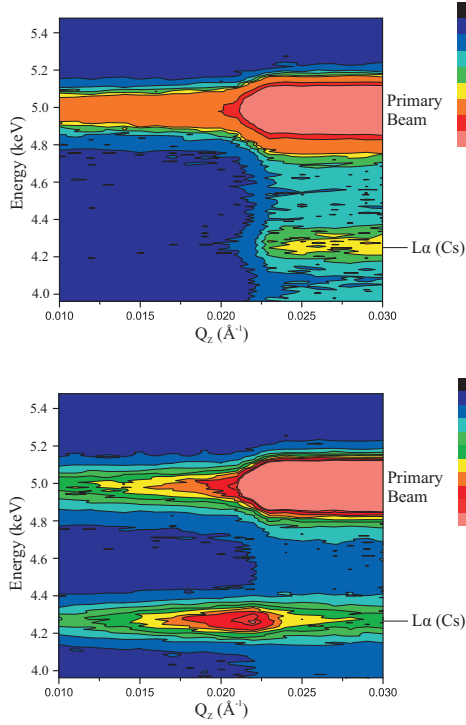


Figure 6: Contour plots of fluorescence intensity for  $10^{-3}$  M CsI without (upper panel) and with monolayer DHDP (lower panel). Incident x-ray beam energy is 5.015 keV.

### B. Evaluating interfacial ion concentration

Above the critical angle, the intensity of the X-ray beam,  $I(z)$ , decays as it penetrates deeper into the sample as follows,  $I(z) = I_0 e^{-z/D(\alpha)}$ , where  $I_0$  is the incident beam intensity and  $D(\alpha)$  is the penetration depth, which is a function of the incident beam angle ( $\alpha$ ) and x-ray energy. Assuming the fluorescence intensity from one ion is  $CI_0$  ( $C$  is a scale factor, determined from the experimental setup), the fluorescence intensity collected by the detector has two contribution from the surface and bulk,  $I_s$  and  $I_b$ , respectively. The surface scattering is given by,

$$I_s = CI_0 A N_{ion} / A_{lipid}, \quad (1)$$

and the bulk scattering is

$$I_b = CI_0 A \rho_{bulk} \int_0^\infty e^{-z/D(\alpha)} dz = CI_0 A \rho_{bulk} D(\alpha), \quad (2)$$

where  $A$  is the detector area,  $N_{ion}$  is the number of ions per lipid,  $A_{lipid}$  is the lipid area (i.e., molecular area), and  $\rho_{bulk}$  is the ion bulk concentration.  $I_b$  can be obtained from the fluorescence data of the pure solution without the monolayer, while  $I_s$  can be obtained from the fluorescence data of the solution with the monolayer after the subtraction of  $I_b$ . Using Eqs. (1) and (2), one can readily get the number of ions per lipid at the

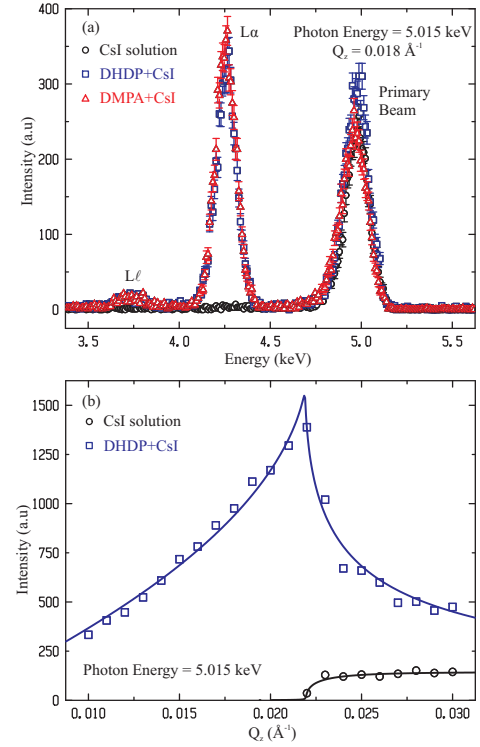


Figure 7: (a) Fluorescence intensity versus emission line energy at  $Q_z = 0.018 \text{ \AA}^{-1}$  with and without monolayer materials ( $E$ -cuts from Fig. 6). (b) Fluorescence intensity of  $\text{Cs}^+$   $L\alpha$  emission line versus  $Q_z$  with and without DHDP ( $Q_z$ -cuts Fig. 6).

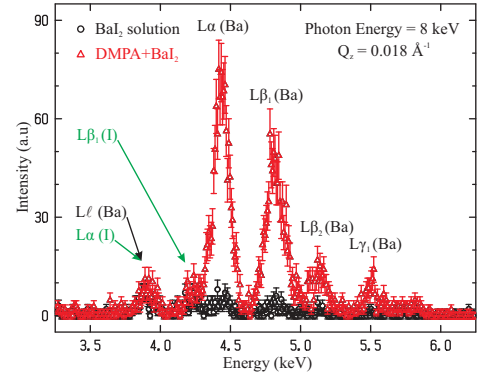


Figure 8: Fluorescence intensity versus emission line energy for  $10^{-2}$  M  $\text{BaI}_2$  with and without DMPA at  $Q_z = 0.018 \text{ \AA}^{-1}$ . Emission lines from both  $\text{Ba}^{2+}$  and  $\text{I}^-$  are labeled.

surface, using the following relation,

$$N_{ion} = \frac{I_s(\alpha)}{I_b(\alpha)} A_{lipid} D(\alpha) \rho_{bulk}. \quad (3)$$

The absorption of emitted photons as they traverse to the EDD is negligible, since their path in the sample is shorter than that of the incident beam by a factor of at least 100.

Figure 9 shows that the fluorescence data, above the critical angle, at  $Q_z = 0.030 \text{ \AA}^{-1}$  for  $10^{-3}$  M CsI with and

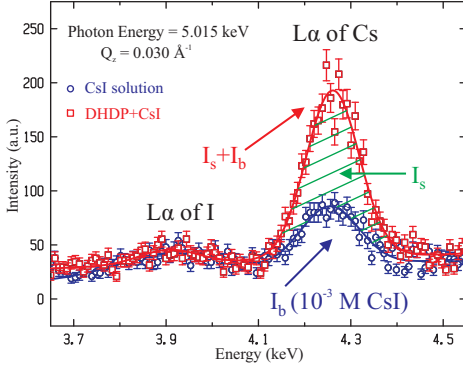


Figure 9: Fluorescence data above the critical angle ( $Q_z = 0.030 \text{ \AA}^{-1}$ ) for  $10^{-3} \text{ M CsI}$  with ( $I_s + I_b$ ) and without DHDP ( $I_b$ ). The shaded area represents  $I_s$  of  $\text{Cs}^+$   $L\alpha$  emission line. X-ray energy is 5.015 keV.

without the monolayer DHDP, and the definition of measured  $I_s$  and  $I_b$ . Spreading a DHDP monolayer enriches the surface with  $\text{Cs}^+$  ions and enhances the  $L\alpha$  emission line (shaded area), but does not change the intensity of  $\text{I}^-$   $L\alpha$  emission line. Some of the emission lines from different ions overlap, due to the poor resolution of the EDD (150 - 200 eV). For instance, the emission line of the  $\text{Cs}^+$   $L\alpha$  line (4.3 keV), and the  $\text{I}^-$   $L\beta_1$  may cause overestimating  $I_b$  from the Cs line. To overcome this problem, we used the PyMca program to fit fluorescent data to obtain the relative contributions of both lines from Cs and I<sup>24</sup>. As shown in Eq. (3), the number of ions can be obtained by evaluating  $I_s$  and  $I_b$  at any  $Q_z$  above the critical angle. In this study,  $I_s$  and  $I_b$  were measured at eight different  $Q_z$  values (from 0.023 to  $0.030 \text{ \AA}^{-1}$ ), yielding an average  $0.47 \pm 0.09$  and  $0.54 \pm 0.09 \text{ Cs}^+$  per lipid for  $10^{-3} \text{ M CsI}$  solution with DHDP and DMPA as a monolayer, respectively. Both values are in an good agreement with anomalous reflectivity<sup>2</sup> and constant- $Q_z$  energy scans<sup>3</sup> studies, where more complicated data analysis is required.

### C. Evaluating the Fine Structure $f''(E)$

The intensity of the emission line is proportional to the absorption of the ion, which is strongly dependent on photon energy near an absorption edge, and also the immediate environment of the ion. By varying the incident beam energy at a fixed  $Q_z$ , we obtain the energy dependence of the absorption correction, namely  $f''(E)$  up to a scale factor. Performing this experiment below the critical angle does not require any geometry or absorption corrections, since there is negligible bulk contribution to the signal as the emitting ions are concentrated at the first  $10 \text{ \AA}$  of the surface<sup>2</sup>.

Figure 10 shows the fluorescence intensity of the  $\text{Cs}^+$   $L\alpha$  emission line as a function of the incident beam energy. DHDP and DMPA were used as monolayer materials,  $Q_z$  was fixed at  $0.018 \text{ \AA}^{-1}$  to minimize the bulk con-

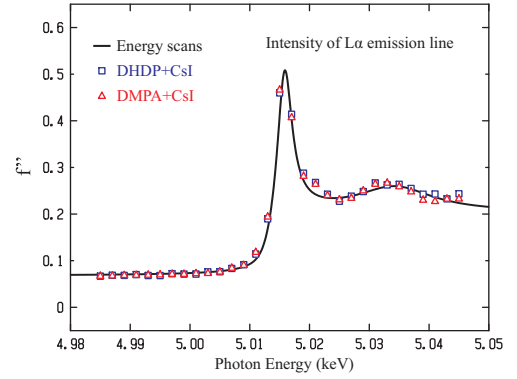


Figure 10: Fluorescence intensity of the  $\text{Cs}^+$   $L\alpha$  emission line from  $10^{-3} \text{ M CsI}$  with the monolayers (DHDP and DMPA) at  $Q_z = 0.018 \text{ \AA}^{-1}$ . The intensity is scaled to the  $f''(E)$  far away from the  $\text{Cs}^+$   $L_{III}$  resonance ( $\pm 30 \text{ eV}$ ). The solid line is  $f''(E)$  obtained by fixed- $Q_z$  energy scans<sup>3</sup>.

tribution. The incident beam energy was scanned around the  $\text{Cs}^+$   $L_{III}$  resonance. Far away from that resonance ( $\pm 30 \text{ eV}$ ),  $f''(E)$  for Cs is known from various experimental and theoretical studies<sup>14</sup>. In the vicinity of the resonance,  $f''(E)$  of the emitting ion can be influenced by the local environment, and the spectra becomes more complex. By scaling the  $f''(E)$  values away from the resonance ( $\pm 30 \text{ eV}$ ), the fluorescence intensity of the  $\text{Cs}^+$   $L\alpha$  emission line can be converted to the specific  $f''(E)$  in its interfacial environment. As shown in Fig. 10, the fluorescence intensity after scaling agrees well with  $f''(E)$ , obtained in our previous study<sup>3</sup> (solid line) by a more complicated analysis of constant- $Q_z$  energy scans. We note that the reported measurement of  $f''(E)$  in bulk aqueous environment (see Fig. 5 in Ref.<sup>13</sup>) is slightly different than the one we report here for the  $\text{Cs}^+$   $L_{III}$  edge. These differences may arise from the fact that the ions in our study reside at the interface with a slightly different environment than that in bulk solution.

## IV. SUMMARY

In the present study we extended previous x-ray fluorescence techniques that had been used to determine the interfacial ion enrichment at charged monolayers<sup>4-10</sup> by tracing all emissions lines that can be resolved by our EDD. Although x-ray fluorescence has been used for detecting the number density of ions of similar systems by similar means, these either needed complicated data analysis<sup>6</sup> or were limited to providing the number density of ions relative to a known density of another ion at the interface<sup>10,19</sup>. We confirmed that the fluorescence technique below the critical angle provides a quick and reliable determination of the presence of ions, specifically by identifying the characteristic emission lines of each element that fluoresce. We demonstrated how to calculate the number density of  $\text{Cs}^+$  ions at the surface by measur-

ing the fluorescence signals with and without the monolayer above the critical angle. We have also shown that the fine structure of the absorption  $f''(E)$  for the specific ions at the surface can be readily obtained from fluorescence signals measured as a function of photon energy near an absorption edge.

The spatial resolution of ion distributions near charged objects (for instance, membranes, DNA filaments, vesicles, polyelectrolytes, and others) in aqueous environment have been improved in recent years with the advances in synchrotron x-ray radiation and have been expanded to more complex systems<sup>25,26</sup>. These experimental tools, together with theoretical advances<sup>27,28</sup>, brought new insight into the nature of ion accumulation near charged interfaces that allow distinguishing between purely electrostatic attraction and ion-specific binding. The fluorescence technique, first introduced by Bloch and coworkers<sup>6</sup>, is yet another independent technique that

can identify enrichment of ions, specifically from mixed salt solutions, and shed light on the local environment of the ions at the interface in a similar manner to the newly introduced fixed- $Q_z$  energy scan near ion resonances method<sup>3,29</sup>.

### Acknowledgments

We thank D. S. Robinson for technical support at the 6-ID beamline. Ames Laboratory and the MUCAT sector at the APS are supported by the U.S. DOE, Basic Energy Sciences, Office of Science, under contract under Contract No. DE-AC02-07CH11358. Use of the Advanced Photon Source was supported by the U. S. Department of Energy, Office of Science, Office of Basic Energy Sciences, under Contract No. DE-AC02-06CH11357.

- 
- <sup>1</sup> W. Bu, D. Vaknin, and A. Travesset, Phys. Rev. E **72**, 060501 (2005).
  - <sup>2</sup> W. Bu, D. Vaknin, and A. Travesset, Langmuir **22**, 5673 (2006).
  - <sup>3</sup> W. Bu, P. J. Ryan, and D. Vaknin, J. Synchrotron Rad. **13**, 459 (2006).
  - <sup>4</sup> J. M. Bloch, M. Sansone, F. Rondelez, D. G. Peiffer, P. Pincus, M. W. Kim, and P. M. Eisenberger, Phys. Rev. Lett **54**, 1039 (1985).
  - <sup>5</sup> J. M. Bloch and W. B. Yun, Phys. Rev. A **41**, 844 (1990).
  - <sup>6</sup> W. B. Yun and J. M. Bloch, J. Appl. Phys. **68**, 1421 (1990).
  - <sup>7</sup> J. Daillant, L. Bosio, J. J. Benattar, and C. Blot, Langmuir, **7**, 611 (1991).
  - <sup>8</sup> N. N. Novikova, S. I. Zheludeva, O. V. Konovalov, M. V. Kovalchuk, N. D. Stepina, I. V. Myagkov, Y. K. Godovsky, N. N. Makarova, E. Y. Tereschenko, L. G. Yanusova, L. G. *et al.*, J. Appl. Crystallogr., **36**, 727 (2003).
  - <sup>9</sup> S. I. Zheludeva, *et al.*, Mater. Sci. Eng., C, **23**, 567 (2003).
  - <sup>10</sup> V. L. Shapovalov, M. E. Ryskin, O. V. Konovalov, A. Hermelink, and G. Brezesinski, J. Phys. Chem. B **111**, 3927 (2007).
  - <sup>11</sup> D. H. Templeton, L. K. Templeton, J. C. Phillips, and K. Hodgson, Acta Cryst A **36**, 436 (1980).
  - <sup>12</sup> K. M. Kemner, D. B. Hunter, W. T. Elam, and P. M. Bertsch, J. Phys. Chem. **100**, 11698 (1996).
  - <sup>13</sup> J.-X. Gao, B.-W. Wang, T. Liu, J.-C., Wang, C.-L. Song, Z. D. Chen, T.-D. Hu, Y.-N. Xie, J. Zhang, and H. Yang, J. Synchrotron Rad. **12**, 374 (2005).
  - <sup>14</sup> D. T. Cromer and D. Libermann, J. Chem. Phys. **53** 1891 (1970).
  - <sup>15</sup> D. Vaknin, P. Krüger, and M. Lösche, Phys. Rev. Lett. **90**, 178102 (2003).
  - <sup>16</sup> B. W. Gregory, D. Vaknin, J. D. Gray, B. M. Ocko, P. Stroeve, T. M. Cotton, and W. S. Struve, J. Phys. Chem. B **101**, 2006 (1997).
  - <sup>17</sup> B. W. Gregory, D. Vaknin, J. D. Gray, B. M. Ocko, T. Cotton, and W. S. Struve, J. Phys. Chem. B **103**, 502 (1999).
  - <sup>18</sup> D. Vaknin, in *Characterization of Materials*, edited by E. N. Kaufmann, **2**, 1027-1047 (John Wiley & Sons, New York, 2003).
  - <sup>19</sup> W. Bu, K. Flores, J. Pleasant, and D. Vaknin, Langmuir **25**, 1068 (2009).
  - <sup>20</sup> A. Travesset and D. Vaknin Europhysics Lett. **74**, 181 (2006).
  - <sup>21</sup> J. Pittler, W. Bu, D. Vaknin, A. Travesset, D. J. McGillivray, and M. Lösche, Phys. Rev. Lett. **97**, 046102 (2006).
  - <sup>22</sup> G. Vineyard, Phys. Rev. B **26**, 4146 (1982).
  - <sup>23</sup> K. Kjaer, Physica B **198**, 100 (1994).
  - <sup>24</sup> PyMca program <http://pymca.sourceforge.net/> is capable of fitting the fluorescence data with fixed ratios of all emission lines for one specific element. According to intensity of  $I^- L\alpha$ , which is not mixed up with any other emission line in our system, the intensity of  $I^- L\beta_1$  can be calculated and further removed from the overlapping region of the  $Cs^+ L\alpha$ .
  - <sup>25</sup> G. M. Luo, S. Malkova, J. Yoon, D. Schultz, G. B. H. Lin, M. Meron, I. Benjamin, P. Vanysek, and M. L. Schlossman, Science **311**, 216 (2006).
  - <sup>26</sup> K. Giewekemeyer and T. Salditt, Euro. Phys. Lett., **79**, 18003/1-18003/6 (2007).
  - <sup>27</sup> P. Koelsch, P. Viswanath, H. Motschmann, V. L. Shapovalov, G. Brezesinski, H. Möhwald, D. Horinek, R. R. Netz, K. Giewekemeyer, T. Salditt, H. Schollmeyer, R. von Klitzing, J. Daillant, and P. Guenoun, Coll. Surf. A **303**, 110 (2007).
  - <sup>28</sup> D. Andelman, Proceedings of the Nato ASI & SUSSP on Soft condensed matter physics in molecular and cell biology, pg. 97-122, ed. by W. Poon and D. Andelman, (Taylor & Francis, New York, 2006).
  - <sup>29</sup> C. Park, P. A. Fenter, N. C. Sturchio, and J. R. Regalbutto, Phys. Rev. Lett., **94**, 076104 (2005).